Journal of Applied Polymer Science

Effect of interfacial pretreatment on the properties of montmorillonite/poly(vinyl alcohol) nanocomposites

Shailesh Shori,[1] Xiaoming Chen,[1] Michael Peralta,[1] Hongsheng Gao,[1] Hans-Conrad zur Loye,[2] Harry J. Ploehn[1]

[1]Department of Chemical Engineering, University of South Carolina, Columbia, South Carolina
[2]Department of Chemistry & Biochemistry, University of South Carolina, Columbia, South Carolina
Correspondence to: H. J. Ploehn (E-mail: Ploehn@cec.sc.edu)

ABSTRACT: This work explores the factors that control the dispersion of exfoliated montmorillonite (MMT) in poly(vinyl alcohol) (PVOH) during solution blending and solvent evaporation. Nanocomposite films were prepared by solution blending of aqueous PVOH solutions with dilute suspensions of fully exfoliated MMT platelets (as confirmed by AFM). Dynamic light scattering (DLS) indicates that addition of MMT suspensions to PVOH solutions results in undesired particle aggregation and thus poor MMT dispersion in cast films (as evidenced by transmission electron microscopic images and gas permeation measurements). We believe that PVOH bridging induces MMT platelet aggregation. To counteract bridging aggregation, we explore the novel idea of pretreating the MMT surface with a small amount of compatible polymer prior to solution blending with PVOH. We hypothesize that "pretreating" the MMT platelet surfaces with adsorbed polymer in dilute suspensions will protect the platelets from bridging aggregation during solution blending and solvent evaporation. MMT/PVOH composite films have been prepared using low-molecular-weight PVOH as the pretreatment polymer; and low-, medium-, and high-molecular-weight PVOH as the matrix polymer. A PEO-PPO-PEO triblock copolymer (F108 from the Pluronics® family) was also evaluated as the pretreatment polymer. DLS shows that pretreated MMT platelets are less susceptible to aggregation during blending with PVOH solutions. Results compare the crystalline structure, thermal properties, dynamic mechanical properties, gas permeability, and dissolution behavior of MMT/PVOH films incorporating untreated versus pretreated MMT. © 2015 Wiley Periodicals, Inc. J. Appl. Polym. Sci. **2015**, *132*, 41867.

KEYWORDS: clay; composites; hydrophilic polymers; properties and characterization; surfaces and interfaces

Received 21 October 2014; accepted 13 December 2014
DOI: 10.1002/app.41867

INTRODUCTION

Polymer nanocomposites (PNCs) are increasingly utilized in automotive, aerospace, energy, and flame retardant applications. PNCs may offer significant performance advantages over traditional polymer composites, including: (1) enhanced physical properties; (2) ability to tailor material properties for new applications; (3) improved performance/weight ratio achieved by reduction of filler loadings from 15 to 40 vol % to as little as 1 to 5%; and, (4) improved processing performance.

Advances in the fundamental understanding of the role of the filler-polymer interface (really an "interphase") have driven growth in PNC applications. As discussed in many reviews of PNC research,[1–18] the interphase has distinct properties that are amplified by the high interfacial area/volume ratio achieved when the filler particles have nanoscale dimensions. The properties of the interphase also control the dispersion state of the nanoparticles in the polymer. Poor nanoparticle dispersion reduces interfacial area and thus the contribution of the interphase to the composite properties. Consequently, achieving enhanced nanocomposite properties and performance depends critically on maximizing nanoparticle dispersion in the polymer.

The challenge lies in overcoming attractive particle–particle interactions responsible for filler aggregation. Considerable research has focused on the design of filler–polymer interphases to maximize nanoparticle dispersion in polymers.[13,14,19–26] For example, early work on clay/polymer PNCs utilized cation exchange treatment of clay minerals with alkylammonium salts to make the clay platelets more hydrophobic and (in principle) more compatible with polymers.[1–5,7,12,16,17] More recent work explores covalent grafting of polymers on particles for tailoring interphase properties and particle dispersion.[19,22–26] Work to date has primarily emphasized tailoring the interphase to

Additional Supporting Information may be found in the online version of this article.

control nanoparticle dispersion in polymers. Less attention has been given to evaluating the "direct" contribution of the particle-polymer interphase to PNC properties.[21,27]

Consider, for example, the well-studied PNC consisting of exfoliated montmorillonite (MMT) platelets dispersed in poly(vinyl alcohol) (PVOH).[28–37] Using a suitable cleaning protocol,[38] aqueous suspensions of fully exfoliated MMT can be prepared without the need for dispersants. PVOH is water-soluble and readily adsorbs onto MMT.[39–45] These facts suggest that MMT and PVOH are naturally compatible. Using the solution-blending method,[28–31,33–37] one should be able to prepare "model" or "ideal" nanocomposites consisting of fully exfoliated MMT platelets randomly dispersed in a PVOH matrix.

In many cases, the barrier properties of "ideal" MMT/PVOH PNCs fall short of what one might expect based on the "tortuous path" model.[46–49] For example, values of water vapor permeability[28] and diffusivity[33] in MMT/PVOH composites (with MMT loadings up to 6 wt %) were found to be about 60% lower than those in pure PVOH. Yeh *et al.*[31] observed that water vapor and oxygen permeabilities in MMT/PVOH PNCs initially decreased with increasing MMT loading, but then increased significantly above 5 wt % MMT. Grunlan *et al.*[34] found the opposite trend: depending on relative humidity, oxygen permeability in MMT/PVOH initially increased with MMT loading, reaching a maximum at about 3 wt %, before decreasing at higher loadings. These observations are not only inconsistent, but also disagree with predictions of various tortuous path models, all of which predict sharp, monotonic decreases in gas permeability with increasing platelet loading. These gas permeation studies reveal that our idealized picture of internal structure in exfoliated PNCs must not be complete.

At least two factors may complicate our picture of how structure develops in MMT/PVOH nanocomposites during solution blending and densification of the parent solutions. First, the dissolved PVOH may induce MMT interplatelet attraction, either through bridging adsorption[39,41,44,45,50–53] or depletion flocculation.[41,50,53,54] Second, PVOH may undergo gelation or demixing during densification, opening up the possibility of MMT partitioning into a preferred phase.[55–57] These factors have not been considered in previous studies of MMT/PVOH nanocomposites.

We have found that exfoliated MMT platelets tend to restack or aggregate at some point during the solution blending and densification processes that transform MMT and PVOH solutions into a solid MMT/PVOH nanocomposite. The objective of this work is to explore the role of MMT platelet interactions on platelet dispersion in MMT/PVOH nanocomposites prepared by solution blending. The first part of this work demonstrates that MMT platelet restacking takes place during the solution blending process. The second part investigates a novel concept, MMT surface "pretreatment" by adsorption of low-molecular-weight homopolymer (PVOH) or block copolymer (F108 Pluronic®) from a dilute solution. This pretreatment may prevent bridging flocculation by blocking the MMT surface before solution blending with the PVOH matrix polymer. We assess the impact of MMT pretreatment on platelet dispersion as well as the thermal, mechanical, and gas barrier performance of MMT/PVOH nanocomposites.

EXPERIMENTAL

Preparation of MMT Suspensions

Stock suspensions of fully exfoliated MMT (Cloisite Na^+, Southern Clay Products) were prepared following our published procedure.[38] Typically, the as-received MMT powder is dispersed at 1.0 wt % in deionized (DI) water, mixed at room temperature for at least 12 h, sonicated for 30 min (Fischer-Scientific FS-28), centrifuged at 4000 rpm (2000 g) for 60 min (fixed-angle Eppendorf 5403 centrifuge), followed by careful decanting of the supernatant suspension. The product suspension typically contains about 0.75 wt % MMT (batch-to-batch values ranging from 0.60 to 0.90 wt %) as measured by dry weight analysis. Our previous AFM study[38] shows that the MMT platelets in these suspensions are essentially fully exfoliated; histograms of MMT platelet thickness and aspect ratio (Supporting Information Figures S1 and S2) can be found in the Supporting Information section.[58]

The stock MMT suspension is used to prepare two kinds of pretreated MMT platelet suspensions as well as PVOH nanocomposite films. To prepare MMT pretreated with low-molecular-weight PVOH (11–31 kDa, 98–99% hydrolyzed, Alfa Aesar, used as received; denoted below as PV_{11}), stock MMT suspension is added drop wise to an aqueous solution of PV_{11} with heating (~90°C) and mixing for at least 60 min. The MMT suspension should be added to the PVOH solution, rather than vice versa, to minimize bridging flocculation. The PV_{11} solution concentration and the volume of added MMT suspension are adjusted so that the mixture contains 0.50 wt % PV_{11}, and that the total solids content (i.e., polymer + MMT) is 64.3% PV_{11} and 35.7% MMT by weight. The latter figure must be taken into account when the PV_{11}-treated MMT (denoted henceforth as PV_{11}MMT) is solution-blended with additional matrix PVOH to prepare nanocomposites with precisely 10.0 wt % MMT loading.

For the second pretreated MMT suspension, we add MMT suspension drop wise to an aqueous solution of F108 Pluronic®, a triblock copolymer surfactant (14,600 Da, BASF, used as received) with at least 60 min mixing at room temperature. Both the central poly(propylene oxide) block (DP = 44)[59] and the two poly(ethylene oxide) end blocks (DP = 141)[60] may adsorb on the MMT surface. The MMT suspension and F108 solution volumes are adjusted so that the mixture has a total solids content of 75% MMT and 25% F108 by weight, with a 0.10 wt % F108 concentration. The F108-treated MMT is denoted henceforth as F-MMT.

Preparation of MMT/PVOH Nanocomposite Films

MMT/PVOH nanocomposite films were prepared using low-, medium-, and high-molecular-weight PVOH: PV_{11}, PV_{95} (95 kDa, 95% hydrolyzed, Acros Organics, used as received), and PV_{205} (205 kDa, 99+% hydrolyzed, Sigma Aldrich, used as received). Aqueous PVOH solutions are prepared by dissolution of PVOH powders in DI water with mixing at 90°C for at least 60 min. To prepare nanocomposites with 10 wt % nonpretreated

MMT, an appropriate volume of stock MMT suspension is added drop wise to the warm PVOH solutions so that the final, blended suspension contains an overall PVOH concentration of 5.0 wt % and (on a solids-only basis) 10.0 wt % MMT and 90.0 wt % PVOH.

Solution blending of pretreated MMT suspensions (PV_{11}MMT or F-MMT) with PVOH solutions proceeds in the same way. Suspensions of pretreated MMT were used as prepared, so one must account for the pretreatment polymer content in the blending process. The volume and concentration of PVOH solution must be adjusted so that the total polymer content (PVOH matrix plus PVOH or F108 carried by the pretreated MMT) is precisely 90 wt % in the final composites. The starting PVOH solution also has a lower initial concentration so that the final blended suspension has a total polymer concentration of about 2.0 wt %. Sample "recipes" are provided in Supporting Information.

Solution casting or drawdown coating was used to make nanocomposite films. Solution cast films were prepared by depositing a known mass of blended suspension onto an aluminum pan and drying in air in an oven at either 40°C or 120°C (annealing). For drawdown coating, typically 3–5 mL of blend suspension was deposited onto a Mylar® sheet (supported by a balanced glass plate underneath) and drawn down using a doctor blade. A Microm II film applicator (Gardco) was configured with a doctor blade gap distance set to 1 mil (25.4 μm) in order to control the thickness of the final film. Sliding the blade slowly forms a wet film coating. The plate is then carefully covered with a shield to minimize settling of dust particles onto the wet film. The drawn films were dried at room temperature for 1 day, gently peeled from the Mylar sheet, dried overnight in a vacuum oven at 60°C, and then stored in a sealed desiccator. The final films typically have a thickness of 20–30 μm as measured using a micrometer (Mitutoyo Digimatic Micrometer MDC-MX, model 293-831).

CHARACTERIZATION METHODS

Transmission Electron Microscopy

Electron microscopy employed a Hitachi H-8000 transmission electron microscope (TEM). To prepare a specimen for TEM observation, it was first trimmed to the shape of the cross-section of a BEEM® conical embedding capsule. After placing the film sample in the capsule center (with the film tip aligned with the capsule tip, tip pointing down), a premixed epoxy resin was slowly poured in to embed the sample. The capsule was closed and the epoxy cured at 80°C for 24 h. After curing, the tip of the formed epoxy block was trimmed to expose the sample tip. The tip was then sectioned into several ~100 nm thin slices using an Ultra 35° diamond knife at room temperature. The floating slices were collected from water using carbon coated steel grids, air dried, then observed by TEM under an accelerating voltage of 200 KeV.

X-ray Diffraction

X-ray diffraction (XRD) utilized a Rigaku Ultima IV diffractometer (Cu Kα radiation, $\lambda = 1.5418$Å). Small angle measurements used an incidence angle (ω) of 0.5°, divergence slit (DS) set at 0.1 mm, and scanned over a 2θ range of 0.2–10°. For wide angle scans (2θ from 2° to 50°), the DS was set at 0.2 mm. For both angular ranges, scans used a step size of 0.05° and a scan speed of 2°/min. XRD samples were prepared by drawdown coating of films directly onto transparent glass slides with drying at room temperature.

Dynamic Light Scattering

Dynamic light scattering (DLS) measurements (DynaPro Titan, Wyatt Instruments and Zetasizer Nano ZS ZEN3600, Malvern Instruments) were used to monitor the size of MMT particles in dilute suspensions. Additional details are provided in Supporting Information. Samples of aqueous MMT suspensions were diluted with DI water to a weight fraction of about 5.0×10^{-6} (Wyatt). Samples of cast films were dissolved in DI water and characterized by DLS (Malvern) to provide an indirect measure of MMT aggregation. Film samples were dissolved via mixing for at least 24 h in DI water at temperatures ranging from room temperature up to 70°C. The MMT weight fraction was approximately 5.0×10^{-5} in these samples. The intensity autocorrelation function was fit using the quadratic cumulants method to determine the z-average translational diffusion coefficient. The Stokes–Einstein equation is then used to compute the equivalent spherical hydrodynamic diameter of the MMT particles.

Thermal Properties

Differential scanning calorimetry (DSC) and thermogravimetric analysis (TGA) were used to evaluate the thermal properties of nanocomposite films. For DSC (Q2000, TA Instruments), approximately 5 mg of sample (cast film dried at 40°C) was tightly packed into a Tzero aluminum pan (TA Instruments) and then sealed. Two identical heating/cooling cycles (40–240°C, 10°C/min scan rate) were conducted under nitrogen purge. For TGA (Q5000, TA Instruments), approximately 8–10 mg of sample (cast film dried at 40°C) was placed onto a high-temperature platinum pan (TA Instruments) and heated in air to 800°C at a scan rate of 10°C/min.

Mechanical Properties

Dynamic mechanical analysis (DMA) was used to characterize nanocomposite mechanical properties (RSA-III, TA Instruments). Samples of drawn films were cut into strips (47–49 mm length, 6–7 mm width, 20–30 μm thickness) and then dried in a vacuum oven at 60°C for 24 h. Specimens were carefully mounted in the tensile testing fixture followed by zeroing the pretension, heated to 140°C, and held at that temperature for 5 min. Complex tensile modulus was measured during a temperature sweep from 140°C to −80°C (−3°C/min ramp rate, 1.0 Hz frequency, 0.05% strain amplitude). At least three specimens of each nanocomposite were tested.

Gas Permeability

The gas barrier properties of nanocomposite films were measured using a custom-built gas permeation system (Figure S3, Supporting Information). The main components of the permeation system are a continuous-flow permeation cell, a variable leak valve, and a quadrupole mass spectrometer (SRS100, Stanford Research Systems). After drying in a vacuum oven at 60°C for at least 24 h, a drawn film was masked on both sides using

heavy-duty aluminum foil sealed with high vacuum grease, leaving exposed a circular area of about 5 cm^2. The masked film was seated and sealed in the permeation cell. One side was exposed to the test gas, water vapor at 36.5°C at >97% relative humidity. A carrier gas (N_2) flowed at a controlled mass flow rate over the other side, carrying the permeate gas into the mass spectrometer for measurement of the permeate concentration. A mass balance yields the water vapor transmission rate (WVTR). For each nanocomposite, WVTR was measured for at least three replicate film specimens.

RESULTS AND DISCUSSION

"Ideal" MMT/PVOH Nanocomposites

Previous research[38] has established purification procedures (described above) that produce suspensions of almost completely exfoliated MMT platelets, as verified by AFM (Figures S1 and S2, Supporting Information). Supporting Information Figure S1 indicates that 98% of the MMT particles are either pristine single platelets or "duplex stacks" consisting of two stacked platelet fragments. AFM also provides accurate quantification of the platelet aspect ratio distribution (Supporting Information Figure S2). The measured aspect ratio distribution may be used in conjunction with a recent version of the tortuous path model[49] to estimate the gas barrier performance of PNC films containing platelets with considerable size polydispersity.

This work began with two initial hypotheses. The first was that "ideal" MMT/PVOH nanocomposites prepared from suspensions of fully exfoliated MMT platelets should exhibit superior gas barrier performance compared to that reported previously.[28,31,33,34] Second, by properly accounting for platelet polydispersity, the tortuous path model[49] should be able to rationalize the measured gas barrier performance of our supposedly "ideal" MMT/PVOH nanocomposites.

To this end, we prepared a series of MMT/PVOH nanocomposite films with varying MMT loadings and measured their oxygen permeabilities. Figure 1 plots this data in terms of the O_2 barrier factor (the O_2 permeability of pure PVOH divided by that of a MMT/PVOH nanocomposite), along with predictions of the tortuous path model[49] based on the MMT platelets' measured aspect ratio distribution (Supporting Information Figure S2). The O_2 barrier factor rises monotonically with MMT loading but falls substantially below the prediction of the tortuous path model for fully exfoliated platelets (curve denoted by $n = 1$). If we use the same aspect ratio distribution but assume that the dispersed particles are aggregated platelet "stacks" with an average of four platelets each (curve denoted as $n = 4$), the model prediction rationalizes the barrier data up to 5 wt % MMT, but significantly overpredicts barrier performance at higher MMT loadings.

The O_2 barrier data and comparisons with model predictions essentially invalidate both of our initial hypotheses. Although the increase in O_2 barrier with MMT loading agrees with expectations, measured barrier performance is not superior to that observed previously. Moreover, the differences between measured and predicted barrier performance indicate flaws in the assumptions of the tortuous path model, flaws in our concept of "ideal" MMT/PVOH nanocomposites (i.e., that we could prepare fully exfoliated PNCs by blending verified, fully exfoliated platelet suspensions with solutions of compatible polymer), or both.

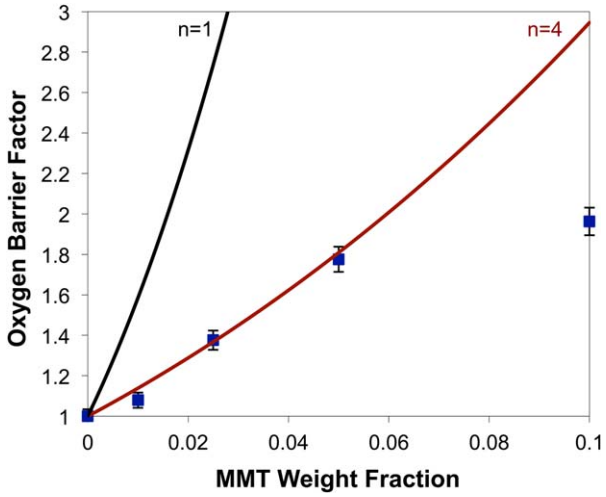

Figure 1. Oxygen barrier factor (symbols) for MMT/PVOH nanocomposites as a function of MMT loading (95 kDa PVOH matrix). The solid curves are calculated via the tortuous path model for polydisperse platelets[49] based on the aspect ratio distribution measured for this MMT by AFM (Figure S2, Supporting Information). Labels denote calculations assuming full exfol-iation ($n = 1$) and partial aggregation into stacks containing an average of four platelets ($n = 4$). [Color figure can be viewed in the online issue, which is available at wileyonlinelibrary.com.]

TEM images give qualitative indications of nonidealities in structure that arise during solution blending, solvent evaporation, and film densification. Away from the surfaces of a 10 wt % MMT/PVOH composite film, we observe regions of what appear to be face-aggregated platelets in addition to regions of well-dispersed, individual platelets [Figure 2(a)]. Other TEM images (Figure S4, Supporting Information) show similar regions in both 1 and 10 wt % MMT/PVOH composites. This shows that although MMT platelets are fully exfoliated in the starting stock suspension, they undergo at least partial aggregation during solution blending, solvent evaporation, and film densification. Near the film surface, we observe what appears to be a wrinkled region of layered, consolidated platelets [Figure 2(b) and Supporting Information Figure S5]. The wrinkling could be caused by stresses generated either during densification or microtoming. Regardless, the observed platelet consolidation should not occur if the densification process only involves water removal from a uniform mixture of PVOH and exfoliated MMT platelets. Both platelet aggregation and surface consolidation provide evidence for some kind of platelet–platelet attraction that arises during solution blending, solvent evaporation, and film densification.

PVOH readily adsorbs onto MMT in water.[39–45] This suggests that PVOH-mediated bridging attraction might lead to MMT aggregation during the solution blending process. DLS data provide some evidence for this. For diluted MMT stock suspensions (MMT, Figure 3), the measured particle size is about

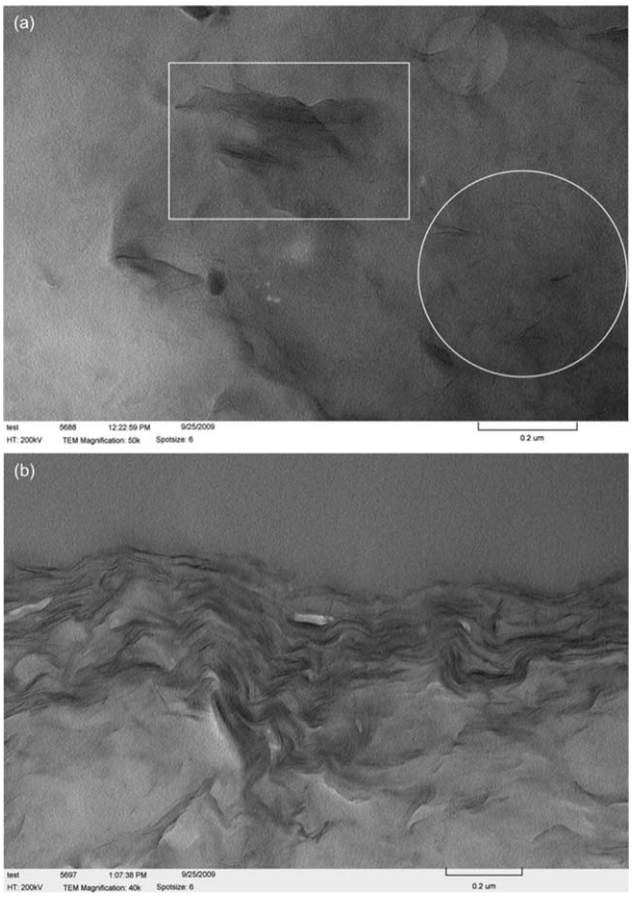

Figure 2. TEM images of a 10 wt % MMT/PV_{95} nanocomposite. (a) Interior region with indicated areas containing well-dispersed platelets (circle) and face-aggregated platelets (rectangle). (b) Surface region showing a wrinkled "skin" of consolidated platelets.

186 ± 9 nm, independent of the MMT concentration after dilution. This DLS particle size agrees well with the platelets' characteristic lateral dimension as measured by AFM (Supporting Information Figure S2). MMT stock suspension was then mixed with PV_{205} solution to produce a blend suspension

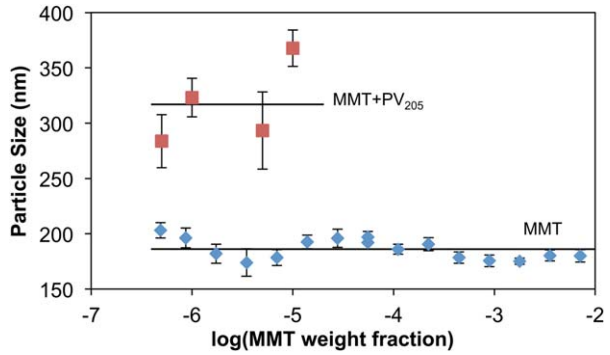

Figure 3. MMT particle size as measured by DLS. MMT: MMT stock suspension diluted to the indicated MMT weight fraction. MMT + PV_{205}: MMT stock suspension mixed with PV_{205} solution to produce a blend suspension containing 0.28 wt % MMT and 5.0 wt % PV_{205}, and then diluted to the indicated MMT weight fraction. [Color figure can be viewed in the online issue, which is available at wileyonlinelibrary.com.]

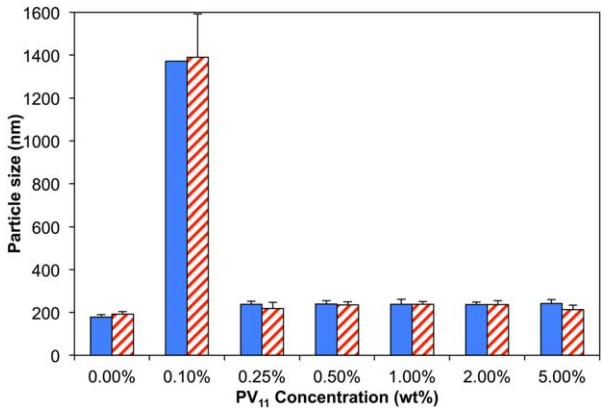

Figure 4. MMT particle size, as measured by DLS, in suspensions containing various concentrations of PV_{11}. Suspensions were diluted with DI water to MMT weight fractions of 1.0×10^{-5} (solid bars) or 5.0×10^{-6} (hatched bars). [Color figure can be viewed in the online issue, which is available at wileyonlinelibrary.com.]

(MMT + PV_{205}, Figure 3) containing about 0.28 wt % MMT and 5.0 wt % PVOH. After dilution to the indicated MMT concentrations, the particle size measured by DLS ranged from 284 to 368 nm (average 317 ± 38 nm) with larger polydispersity indices. The greater particle size (compared to the starting MMT) results from a combination of PVOH adsorption and platelet aggregation due to polymer bridging.

MMT Platelet Pretreatment

The previous results lead to the third hypothesis investigated in this work: that initially coating MMT platelets with a protective layer of polymer may reduce bridging attraction between platelets, promote better platelet dispersion, and improve the properties of MMT/PVOH nanocomposites. We refer to this preliminary coating as "pretreatment," considering that the platelets will subsequently undergo blending with PVOH matrix polymer and then densification to form MMT/PVOH nanocomposites.

To test this hypothesis, we seek a pretreatment polymer that readily adsorbs onto MMT, has good compatibility with the PVOH matrix, and does not itself produce bridging aggregation. High-molecular-weight PVOH (such as PV_{205}) should adsorb strongly and provide a thick steric barrier, but it also may promote bridging aggregation (Figure 3). For this reason, we focused on two lower molecular weight pretreatments: PV_{11} and F108 Pluronic®, a PEO-PPO-PEO triblock copolymer. The polymer concentration used in pretreatment should maximize adsorption and thus the effectiveness of the steric barrier. On the other hand, if the pretreatment polymer concentration is too high, then its concentration in the final polymer nanocomposite will be too high, as well (see Supporting Information for details).

MMT was pretreated with PV_{11} by adding MMT stock suspension to PV_{11} solutions, producing PV_{11}MMT suspensions with varying PV_{11} concentration. The MMT particle size was measured by DLS after dilution with DI water (Figure 4). For the pretreatment suspension containing 0.1 wt % PV_{11}, the large apparent particle size clearly indicates MMT aggregation. In this

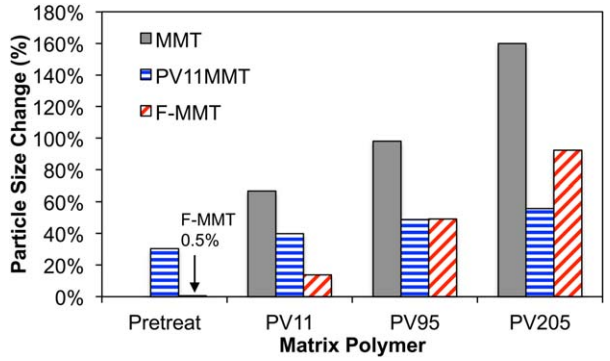

Figure 5. Percentage change in apparent particle size (relative to untreated MMT in stock suspension) for particles in pretreatment suspensions ("pretreat") and MMT + PVOH blend suspensions (2 wt % polymer) with various PVOH molecular weights (PV_{11}, PV_{95}, and PV_{205}). The legend indicates results for untreated MMT and pretreated PV_{11}MMT and F-MMT. All samples for DLS were diluted with DI water to an MMT weight fraction of 5.0×10^{-6}. [Color figure can be viewed in the online issue, which is available at wileyonlinelibrary.com.]

case, PV_{11} acts as a flocculent: the low concentration results in reduced amount of adsorbed polymer.[41,45] Previous research[51,61–63] clearly indicates very low polymer adsorbed amounts result in only partial coverage of the MMT surface, which may enable PV_{11} bridging that leads to MMT aggregation. For PV_{11}MMT suspensions with 0.25 wt % and higher PV_{11} concentrations, the MMT particle size is consistently about 25% higher than that in the MMT stock suspension. As in the case of MMT + PV_{205} (Figure 3), the larger effective particle size may be due to a combination of PV_{11} adsorption (producing larger hydrodynamic drag on the diffusing PV_{11}MMT platelets) as well as low levels of MMT aggregation. However, the higher PV_{11} concentrations clearly do not result in large-scale MMT flocculation. Additional light scattering characterization of F108, PV_{95}, and PV_{205} pretreatment suspensions may be found in Supporting Information (Figure S6).

Among the PV_{11} solutions listed in Figure 4, the pretreatment suspension containing 0.50 wt % PV_{11} was selected for preparing nanocomposites in subsequent solution blending. Depending on the MMT weight fraction in the starting MMT stock suspension, this pretreatment suspension typically contained 30–40 wt % MMT (on a solids basis) with the balance as PV_{11}. These quantities must be taken into account in subsequent solution blending to achieve the target MMT loading (10.0 wt %) in the final composite (see Supporting Information for details).

Next, we assess the extent to which pretreatment using PV_{11} or F108 prevents polymer bridging during solution blending. Figure 5 shows the effect of solution blending on the apparent size of MMT particles, expressed as percentage change relative to the MMT particle size in the starting stock suspension for each set of experiments. For the pretreatment suspensions, the average particle sizes in PV_{11}MMT and F-MMT are about 30% and 0.5% greater, respectively, than that in MMT stock suspension. This may indicate some bridging aggregation in PV_{11}MMT suspension, which is not observed in F-MMT suspension.

Blending untreated MMT stock suspensions with PVOH solutions results in significant increases in apparent particle size, ranging from 67% for MMT + PV_{11} to 160% for MMT + PV_{205}. This indicates a strong tendency of PVOH to induce bridging aggregation of untreated MMT, which increases with polymer molecular weight. For pretreated PV_{11}MMT suspension blended with PVOH solutions, the particle size only increases from 40% to 56% with increasing PVOH molecular weight. Thus, PV_{11} pretreatment seems to reduce the incidence of bridging aggregation during solution blending of PV_{11}MMT suspension with PVOH solutions. The dependence on the PVOH molecular weight is weak. Although thermodynamically favored, PV_{95} and PV_{205} do not displace previously adsorbed PV_{11} from the MMT surface on the time scale of these experiments.

We observe a similar trend for solution blending of pretreated F-MMT suspension with PVOH solutions, but the molecular weight dependence is more pronounced (14%, 49%, and 92% particle size increase upon blending F-MMT with PV_{11}, PV_{95}, and PV_{205} solutions, respectively). We infer that PV_{11} does not readily displace "preadsorbed" F108 from the surfaces of F-MMT platelets. On the other hand, higher molecular weight PV_{205} appears to be more effective at displacing F108 from the F-MMT surface, resulting in a higher incidence of bridging aggregation. Overall, these results suggest that F108 may be preferable for pretreating MMT to prevent bridging if the molecular weight of the PVOH matrix is low. If the molecular weight of the PVOH matrix is high, then PV_{11} is preferable for preventing MMT bridging aggregation during solution blending.

MMT/PVOH Nanocomposite Properties

Structural Characterization. XRD measurements provide information on structure within MMT/PVOH nanocomposites, including the effect of MMT on PVOH crystallinity and the incidence of platelet restacking. Figure 6 shows XRD patterns for the starting MMT powder, neat PV_{95} film, and various 10 wt % MMT/PV_{95} composites. Additional plots for neat PV_{11}

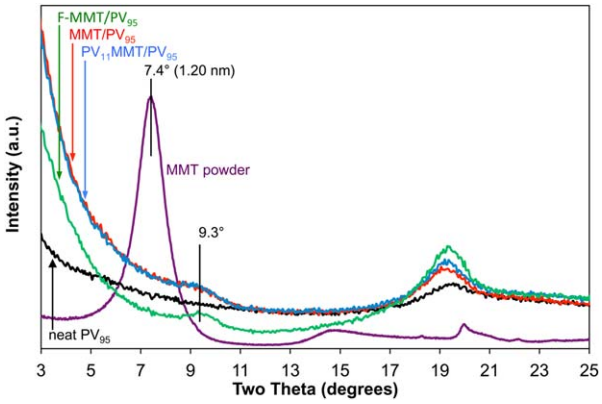

Figure 6. XRD patterns for starting MMT powder, neat PV_{95} film, and various 10 wt % MMT/PV_{95} composites as labeled in the plot. The intensity upturn at low angles is due to the underlying glass slide used to mount the polymer films for XRD. [Color figure can be viewed in the online issue, which is available at wileyonlinelibrary.com.]

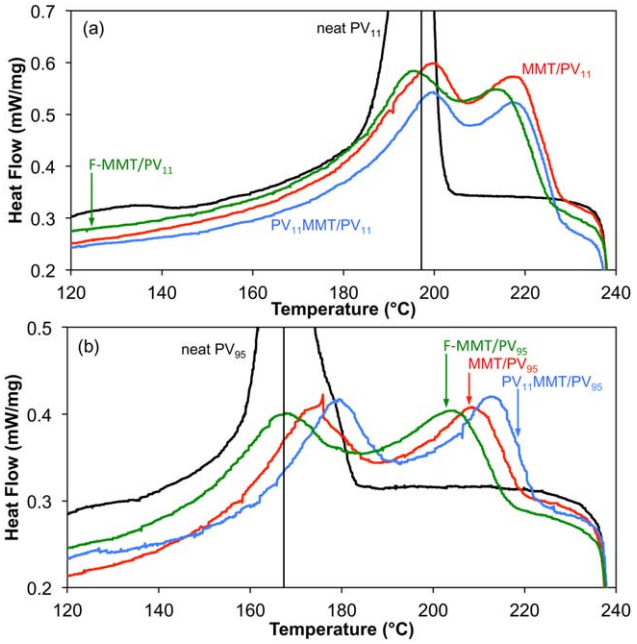

Figure 7. Exothermic heat flow during DSC first cooling scans for: (a) neat PV_{11} film and various MMT/PV_{11} composites and (b) neat PV_{95} film and various MMT/PV_{95} composites. The solid vertical lines indicate the locations of maxima in the crystallization peaks for the neat PV_{11} and PV_{95} films. [Color figure can be viewed in the online issue, which is available at wileyonlinelibrary.com.]

and PV_{205} films and their MMT nanocomposites may be found in Supporting Information (Supporting Information Figures S7 and S8). The pattern for MMT powder features a prominent (001) peak centered at 7.38°, corresponding to a layer spacing of 1.20 nm, as expected. The pattern for neat PV_{95} film has a broad peak centered at 19.6° that is typically associated with semicrystalline PVOH structure.[28,29,32,37] The patterns for all of the MMT/PVOH nanocomposites (Figure 6) are similar. First, none of the composite patterns show evidence of a peak near 7.4° associated with the layered MMT structures, nor any peaks at lower angles due to expanded or restacked MMT platelets. All of the composite patterns display weak peaks centered near 9.3°, which we believe to be associated with surface-induced nucleation of additional PVOH crystallites. This peak has been observed previously,[37,45,64] but (in one case) misinterpreted in terms of MMT layer expansion.[37] Our observations suggest that composites prepared with pretreated MMT probably have structures similar to that seen in untreated MMT/PVOH composites.

Thermal and Mechanical Properties. DSC characterization indicates the effect of MMT surface pretreatment on composite thermal properties. DSC results (Figure 7) show that addition of untreated MMT to PVOH nucleates a new crystalline phase with a higher melting temperature than that of the neat polymer.[28] This new crystalline phase forms at the MMT/PVOH interface, accompanied by reduced bulk polymer crystallinity.[29] Our results indicate that MMT surface pretreatment has some effect on nanocomposite crystallinity. For the lowest molecular weight PV_{11} matrix [Figure 7(a)], composites incorporating $PV_{11}MMT$ and untreated MMT have essentially the same crystallization curves; this might be expected since the pretreatment and matrix polymers are the same in the $PV_{11}MMT/PV_{11}$ composite. The crystallite melting temperatures are about 5°C lower for the $F\text{-}MMT/PV_{11}$ composite compared to MMT/PV_{11}. It also appears that the $F\text{-}MMT/PV_{11}$ composite has more bulk and less interfacial crystallinity than MMT/PV_{11}. These observations suggest that adsorbed F108 disrupts the nucleation and growth of interfacial crystallites in the $F\text{-}MMT/PV_{11}$ composite.

For composites based on the intermediate molecular weight PV_{95} matrix [Figure 7(b)], MMT pretreatment with PV_{11} or F108 does not change the total amount of crystallinity or the relative amounts of bulk and interfacial crystallites. However, the nature of the pretreatment has an effect on crystallite nucleation. The $PV_{11}MMT/PV_{95}$ and $F\text{-}MMT/PV_{95}$ composites have crystallization temperatures that are about 5°C higher and 5°C lower, respectively, than those of untreated MMT/PV_{95}. As found for the $F\text{-}MMT/PV_{11}$ composite, the F108 pretreatment appears to disrupt crystallite nucleation in the $F\text{-}MMT/PV_{95}$ composite. In contrast, PV_{11} pretreatment appears to promote PV_{95} crystallite nucleation in the $PV_{11}MMT/PV_{95}$ composite.

The highest PVOH molecular weight used in this study, PV_{205}, is less crystalline than PV_{11} and PV_{95}. Blending untreated MMT with PV_{205} appears to reduce the overall crystallinity in the MMT/PV_{205} composite compared to neat PV_{205} film (Figure 8), but exotherms associated with both bulk and interfacial crystallization are observed in the DSC cooling curve. Compared with the MMT/PV_{205} composite, those prepared with both $PV_{11}MMT$ and F-MMT appear to have higher levels of interfacial crystallization and suppression of bulk polymer crystallization. Enhancement of interfacial crystallization seems to be greater in the $PV_{11}MMT/PV_{205}$ composite.

The effect of MMT pretreatment on composite thermal stability and decomposition rate has been evaluated by TGA (Figures S9–S11, Supporting Information). In all cases, the neat PVOH films and MMT/PVOH composites lose 3–5% of their mass upon heating to 200°C. The composites incorporating $PV_{11}MMT$ appear to have somewhat smaller levels of water loss [Supporting Information Figures S9(a) and S10(a)]. However, the differences are not significant; measured mass losses vary

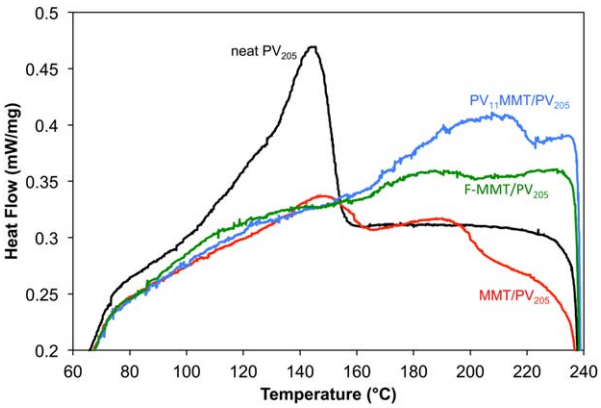

Figure 8. Exothermic heat flow during DSC first cooling scans for neat PV_{205} film and various MMT/PV_{205} composites. [Color figure can be viewed in the online issue, which is available at wileyonlinelibrary.com.]

±3% in this temperature range. The rate of mass loss accelerates at about 260°C for neat PV_{11} and all composites based on PV_{11}. Likewise, the rate of mass loss accelerates at about the same temperature (~290°C) for neat PV_{95} and its composites, as well as neat PV_{205} and its composites (~280°C). At higher temperatures, the presence of MMT slows down the thermal decomposition rates of the composites compared to the corresponding neat polymer films: the increasing MMT content creates a barrier that hinders the escape of decomposition products. However, we observe no significant influence of MMT pretreatment on decomposition rate, compared to composites based on untreated MMT. These TGA observations show that MMT pretreatment has little effect on the thermal stability and decomposition rate of MMT/PVOH composites.

The effect of MMT pretreatment on composite mechanical properties, namely storage modulus and loss tangent, has been evaluated via DMA (Figures S12–S16, Supporting Information). For all matrix PVOH molecular weights, blending untreated MMT with PVOH appears to increase storage modulus (E') at all temperatures, relative to the neat polymer [Figures S12(a) and S13]. Considering values measured at 25°C, average E' values in untreated MMT/PVOH composites are about 13, 42, and 41% higher compared to neat films of PV_{11}, PV_{95}, and PV_{205}, respectively (Supporting Information Figure S14), but the increases are statistically significant only for PV_{95} and PV_{205}. There are no statistically significant differences among the average E' values for composites incorporating untreated MMT, PV_{11}MMT, and F-MMT for all matrix PVOH molecular weights.

With regard to loss tangent [Supporting Information Figure S12(b)], blending untreated MMT or PV_{11}MMT with PV_{95} significantly reduces the magnitude of the loss tangent peak and shifts the peak temperature downward by about 4°C, relative to the corresponding neat PV_{95}. Similar trends in loss tangent peak values are observed for neat polymer films and treated/untreated composites based on PV_{11} and PV_{205} (Figure S15, Supporting Information). Downward shifts of the peak temperature are significant for all fillers for the PV_{11} matrix, and for untreated MMT and PV_{11}MMT for the PV_{95} matrix (Supporting Information Figure S16). Aside from these observations, there are no other statistically significant differences among the average loss tangent peak values or the peak temperatures for composites incorporating untreated MMT, PV_{11}MMT, and F-MMT (Supporting Information Figures S15 and S16). Overall, the DMA results indicate that MMT pretreatment has little or no effect on the mechanical properties of MMT/PVOH composites.

Gas Barrier Performance. The effect of MMT pretreatment on the gas barrier performance of MMT/PVOH nanocomposites was investigated by measurements of WVTR, expressed in Figure 9 as water permeability. Compared to oxygen permeation experiments used in our preliminary work (Figure 1), water permeation tests are much faster, more reproducible, and less sensitive to variations in test gas humidity. Water permeation testing employed the same experimental apparatus as described earlier (see Supporting Information).

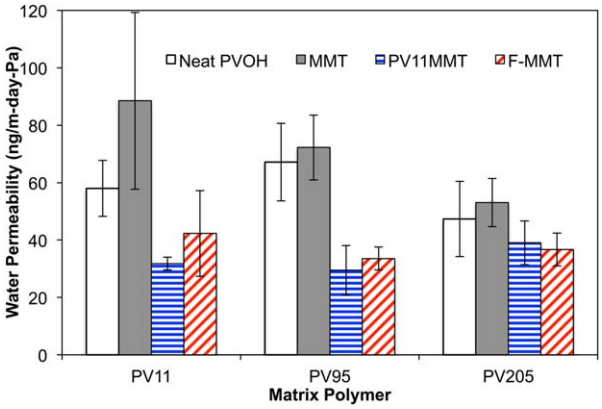

Figure 9. Water permeabilities in PVOH and MMT/PVOH films of low-, medium-, and high-molecular-weight polymer (PV_{11}, PV_{95}, and PV_{205}). Within each group, bars from left to right denote results for neat PVOH and composites incorporating untreated MMT, PV_{11}MMT, and F-MMT. Error bars are 95% confidence limits. [Color figure can be viewed in the online issue, which is available at wileyonlinelibrary.com.]

Each group of bars in Figure 9 compare water permeabilities through films composed of the same molecular weight of the PVOH matrix (neat films and composites). For all PVOH molecular weights, there is no significant difference (at the 95% confidence level) between the permeabilities of untreated MMT/PVOH composites and the corresponding neat PVOH film. For the low-molecular-weight PV_{11} matrix, the untreated MMT/PV_{11} composite has higher water permeability than the neat polymer films at the 86% confidence level. We conclude that for MMT/PVOH composite films made by solution blending, addition of 10 wt % untreated MMT does not improve water barrier performance, and may even increase water permeability relative to neat polymer. This may be explained in terms of untreated MMT's hydrophilic surface: when blended with more hydrophobic PVOH, MMT's hydrophilic surface may provide a more facile pathway for water transport through the polymer matrix.

Considering composites prepared with pretreated MMT, Figure 9 shows that films incorporating either PV_{11}MMT or F-MMT have reduced water permeability values relative to neat PVOH and untreated MMT/PVOH composites. The statistical confidence levels for this observation vary among the data sets. For the lower and intermediate molecular weight PV_{11} and PV_{95} matrix polymers, permeability values for films with pretreated MMT are lower than those for the corresponding neat PVOH and untreated MMT/PVOH composites with greater than 95% confidence levels. The exception among these is F-MMT/PV_{11} compared to neat PV_{11}: the former has a lower permeability with 82% confidence.

For the high-molecular-weight PV_{205} matrix polymer, the trend is the same, but with lower levels of statistical confidence. The average water permeability values of PV_{11}MMT/PV_{205} and F-MMT/PV_{205} composite films are lower than that of untreated MMT/PV_{205} with greater than 90% confidence, and lower than that of neat PV_{205} film with 70–80% confidence. For all three PVOH molecular weights, we observe no significant difference

in water permeability values between PV_{11}MMT and F-MMT composites.

The results for PV_{11}MMT-based composites are particularly remarkable. Pretreating MMT with PV_{11}, and then blending this suspension with the identical PV_{11} as the polymer matrix, produces a composite film with approximately one-third the water permeability (or threefold barrier improvement) compared to a composite film prepared simply by blending untreated MMT with PV_{11} matrix. The composite compositions are identical, but the preparation process varies, with profound consequences on a macroscopic property, water permeability.

Moreover, this unambiguously illustrates the distinct influence of polymer/platelet interfacial nanostructure on a macroscale composite property (water permeability). For adsorption of low-molecular-weight PV_{11} onto MMT from dilute solutions (as in the pretreatment process), PV_{11} molecules adsorb primarily in flattened "train" configurations[51] with most segments contacting the MMT surface. Such adsorbed PV_{11} layers are thin but have high surface coverage; the high areal coverage and flattened polymer configuration on the surface minimize the incidence of bridging aggregation during pretreatment. In contrast, adsorption of PV_{11} from much higher concentration solutions (as in the blending process) results in more extended "loop" and "tail" configurations that leave more of the MMT surface exposed.[51,61–63] If the hydrophilic MMT surface (essentially a defect in the polymer matrix) facilitates water transport in MMT/PVOH composites, then the high MMT surface coverage resulting from PV_{11} pretreatment may be effective in blocking interfacial water transport, thus reducing water permeability relative to that in untreated MMT/PVOH composites.

The overall conclusion is that MMT pretreatment with either PV_{11} or F108 results in composite films with improved water barrier performance compared to composites containing untreated MMT, as well as compared to pure polymer films. This appears to be especially significant for composites made with low to moderate-molecular-weight PVOH matrices. In general, the results suggest that polymer interfacial nanostructure plays a significant, explicit role in water transport in MMT/PVOH composites.

Film Dissolution Behavior. Film dissolution behavior was studied by suspending pieces of composite films in DI water with stirring and modest heating, followed by dilution with DI water and DLS measurement of the average particle size. Consider (1) an "ideal" nanocomposite in which the matrix polymer adheres strongly to the filler nanoparticles, and (2) dissolution utilizing excess solvent that readily solubilizes the polymer and forms stable suspensions of redispersed filler nanoparticles. The particles released from the dissolved film ought to be somewhat larger than the starting filler nanoparticles, with the incremental size increase due to the hydrodynamic effect of adsorbed polymer. In practice, the difference between the final and the initial nanoparticle size may be quite large due to incomplete dissolution, i.e., incomplete polymer-particle deaggregation. Sufficient dilution can eliminate the possibility of large particle aggregates due to depletion flocculation. Assuming that thermodynamics favors complete polymer dissolution and particle redispersion,

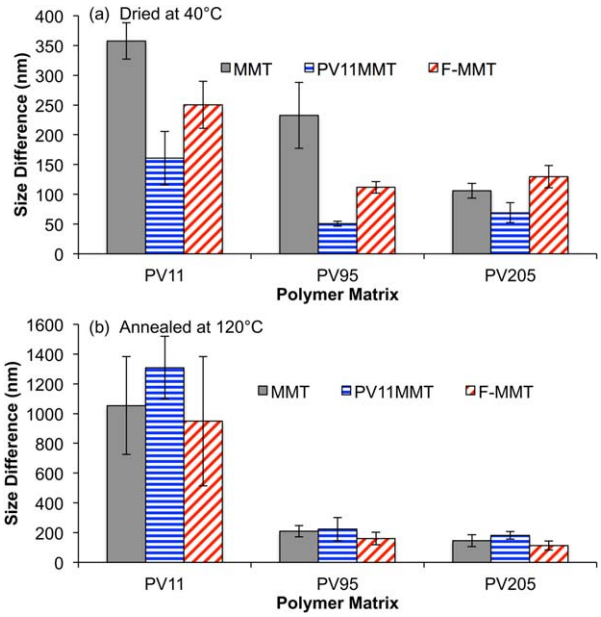

Figure 10. Particle size difference (relative to MMT particle size in stock suspension, measured by DLS) for MMT particles released from MMT/PVOH composite films dissolved in DI water. (a) Film samples dried at 40°C. (b) Film samples annealed at 120°C. Category labels indicate low-, medium-, and high-molecular-weight polymer matrix (PV_{11}, PV_{95}, and PV_{205}). Within each group, bars from left to right denote results for composites incorporating untreated MMT, PV_{11}MMT, and F-MMT. Error bars are 95% confidence limits. In all cases, the dissolved film suspensions were diluted to a MMT weight fraction of 5.0×10^{-5} in DI water. [Color figure can be viewed in the online issue, which is available at wileyonlinelibrary.com.]

the root cause of incomplete dispersion probably lies in polymer-mediated bridging interactions between particles.

The MMT/PVOH system should be "ideal": PVOH is water-soluble, fully exfoliated MMT suspensions can be prepared, and PVOH strongly adsorbs onto MMT. DLS results presented earlier (Figure 5) show that polymer bridging may occur during solution blending of untreated MMT suspensions with PVOH solutions. However, pretreatment with low-molecular-weight PVOH (PV_{11}) or F108 mitigates polymer bridging, at least in part, during solution blending. The film dissolution study aims to characterize, at least qualitatively, the effect of MMT pretreatment on polymer bridging during the film densification and drying steps.

To this end, we prepared solution-cast film samples that were dried, redissolved in DI water, diluted to a predetermined MMT weight fraction, and then characterized by DLS. Two drying protocols were investigated. In the first, the cast films were air-dried in an oven at 40°C. The resulting "dried" films still contained significant amounts of residual water, approximately 2–4 wt % based on TGA data [Figures S9(a)–S11(a), Supporting Information]. In the second drying protocol, the cast films were "annealed" by air-drying in an oven at 120°C, reducing the water content of the films to about 1 wt % or less (estimated from TGA data).

Figure 10(a) shows DLS particle size measurements for suspensions produced by dissolving MMT/PVOH composite films that

had been dried at 40°C. In all cases, the size difference values show that none of the films had undergone complete, "ideal" dissolution into constituent dissolved PVOH and resuspended MMT particles. Considering the untreated MMT/PVOH composites first, the particle size difference decreases as the molecular weight of the PVOH matrix increases. For the highest molecular weight PV_{205} matrix, the density and thickness of the adsorbed steric barrier may be sufficient to minimize aggregation due to polymer bridging and van der Waals attraction. Film dissolution releases individual MMT platelets and small aggregates that may have been present in the blending suspension; hence the measured size difference is relatively small.

For the untreated MMT/PV_{95} and MMT/PV_{11} composites, the polymer adsorbed amount (molecules per unit MMT surface area) and adsorbed layer thickness decrease with decreasing PVOH molecular weight.[51,61–63,65] Thinner adsorbed polymer layers permit closer interactions among MMT platelets in consolidated films, resulting in increased polymer bridging and van der Waals attraction. Upon immersion in water, the MMT aggregates do not disperse as thoroughly, resulting in measured particle size differences that increase with decreasing PVOH matrix molecular weight [Figure 10(a)].

Pretreating MMT with PV_{11} or F108 has a remarkable effect on film dissolution behavior [Figure 10(a)]. For PV_{11}MMT/PV_{11}, the average size of particles released from the dissolved film is almost 200 nm smaller than that of particles released from the dissolved, untreated MMT/PV_{11} composite. In other words, if one pretreats MMT with PV_{11} and then blends this suspension with identical PV_{11} as the matrix polymer, the resulting film dissolves more completely than films prepared by simply blending untreated MMT with PV_{11}.

This observation can be rationalized, once again, in terms of the nanoscale polymer structure at the MMT/PVOH interface. During MMT pretreatment, PV_{11} molecules adsorbing from dilute solution assume flattened "train" configurations. This results in high coverage of the MMT surface, making aggregation due to polymer bridging less likely. Moreover, during solution blending, incoming PV_{11} matrix molecules are less likely to adsorb on the pretreated PV_{11}MMT surface, further mitigating polymer bridging aggregation. The PV_{11} matrix still maintains a steric barrier between nearby MMT platelets. Thus, upon PV_{11}MMT/PV_{11} film dissolution, the released particle aggregates are smaller than those released from dissolved, untreated MMT/PV_{11}. During blending of untreated MMT with higher concentrations of PV_{11} solution, PV_{11} molecules adsorb in more extended "loop/tail" configurations. This surface structure permits more polymer bridging between neighboring platelets during film densification, and thus less complete dissolution when the final film is exposed to water.

Considering the treated F-MMT/PV_{11} composite [Figure 10(a)], particles released during film dissolution are only about 100 nm smaller than those released from the untreated MMT/PV_{11} composite, and about 100 nm larger than particles released from the treated PV_{11}MMT/PV_{11} composite. This implies that F108 does not protect the MMT surface against PV_{11} bridging as effectively as preadsorbed PV_{11}. This again can be rationalized in terms of interfacial structure. F108 is a triblock copolymer that may adsorb onto MMT in a more extended configuration than PV_{11}, making the MMT surface more accessible to incoming matrix PV_{11} molecules during the blending process.

The film dissolution behavior seen for composites based on PV_{11} matrix polymer also applies to PV_{95} composites [Figure 10(a)]. Particles released during the dissolution of PV_{11}MMT/PV_{95} and F-MMT/PV_{95} composites are about 180 nm and 120 nm smaller, respectively, than particles released during the dissolution of MMT/PV_{95} composite. In fact, the particles released by the dissolution of PV_{11}MMT/PV_{95} film are only 50 nm larger than that of the starting MMT platelets used in the composite's synthesis. These results show that PV_{11} and F108 are both effective pretreatments for mitigating polymer bridging during densification of PV_{95}-based composites.

In contrast, PV_{11} and F108 pretreatments do not have much impact on the film dissolution behavior of composites based on the higher molecular weight PV_{205} matrix polymer [Figure 10(a)]. The relatively small particle size difference for untreated MMT/PV_{205} (about 100 nm relative to the starting MMT platelet size) indicates that PV_{205} adsorption onto untreated MMT produces a steric barrier thick enough to significantly reduce polymer bridging during film densification. MMT pretreatment with PV_{11} and F108 does not have much impact, possibly due to the displacement of these lower molecular weight molecules during adsorption of higher molecular weight PV_{205}.

Figure 10(b) shows DLS particle size measurements for suspensions produced by dissolution of MMT/PVOH composite films annealed at 120°C. For composites based on low-molecular-weight PV_{11} matrix polymer, DLS results show that the particles released by film dissolution are more than 1000 nm larger than the starting MMT platelets. Moreover, MMT pretreatment has no significant impact on film dissolution behavior. In practice, these films do not easily dissolve in water, even with extended stirring and heating. For the higher molecular weight PV_{95} and PV_{205} matrix polymers, the released particles are 115–225 nm larger than the starting MMT platelets, indicating more facile film dissolution in these cases. Once again, however, we observe that MMT pretreatment has no significant impact on film dissolution behavior.

These observations can also be rationalized in terms of MMT/PVOH interfacial structure and its dependence on PVOH molecular weight. TGA shows that heating MMT/PVOH composites from 40 to 120°C results in weight losses of 2–4% [Figures S9(a)–S11(a), Supporting Information], almost certainly due to the removal of residual water. Much of this water probably came from the vicinity of the surfaces of the hydrophilic MMT platelets. The residual water occupied space on the MMT surfaces and associated with PVOH molecules, presumably through hydrogen bonding. Removal of the residual water certainly resulted in significant changes in the polymer's interfacial structure, primarily consolidation of the adsorbed polymer layers due to additional binding to the MMT surface. For low-molecular-weight PV_{11} matrix polymer, this leads to MMT platelet–platelet adhesion due to both polymer bridging and van der Waals attraction, making it very difficult to deaggregate and

redisperse the MMT. On the other hand, the higher molecular weight PV_{95} and PV_{205} matrix polymers adsorb to form thicker layers on MMT. Even when the residual water is removed, the thicker steric barriers help mitigate both polymer bridging and van der Waals attraction, making it easier to deaggregate and redisperse the MMT platelets.

CONCLUSIONS

In this work, a low-molecular-weight PVOH (PV_{11}) and a PEO-PPO-PEO triblock copolymer (F108 Pluronic®) were studied as pretreatments to modify the surface of exfoliated MMT platelets prior to solution blending with PVOH matrices of varying molecular weight. DLS (Figure 5) shows that pretreating MMT with PV_{11} or F108 limits platelet aggregation during solution blending, especially as matrix PVOH molecular weight increases. XRD gave no indication of MMT platelet restacking or any variations in polymer crystallinity due to MMT pretreatment. DSC revealed that PV_{11}MMT seemed to promote interfacial nucleation of matrix PVOH, while F-MMT seemed to generally have the opposite effect. Both TGA and DMA suggested that MMT pretreatment had no significant effect on composite thermal stability and mechanical properties, respectively.

On the other hand, MMT pretreatment does have a significant impact on water permeation in MMT/PVOH nanocomposites (Figure 9). By occupying polar water binding sites on the hydrophilic MMT surface, PV_{11} and F108 may impede water transport along the MMT surface, thus enhancing barrier performance. Film dissolution studies also show that MMT pretreatment also influences the dissolution behavior of partially dried, nonannealed MMT/PVOH composite films. Both the water barrier and film dissolution results show that the local nanostructure at the PVOH-MMT interface may be altered by pretreatment with PV_{11} and F108, producing significant changes in macroscopic properties. Direct comparison of results for PV_{11}MMT/PV_{11} and untreated MMT/PV_{11} show that even though the composite compositions are identical, variations in processing details can have a major impact on composite properties and performance. These observations may be significant for polymer nanocomposite applications in the packaging industry.

ACKNOWLEDGMENTS

Financial support for this research was provided by the National Science Foundation (Award IIP-0650186) and the University of South Carolina Office of Research. We thank Dr. Arief Wibowo and Dr. W. Michael Chance for assistance with XRD measurements.

REFERENCES

1. LeBaron, P. C.; Wang, Z.; Pinnavaia, T. *J. Appl. Clay Sci.* **1999**, *15*, 11.
2. Schmidt, D.; Shah, D.; Giannelis, E. P. *Curr. Opin. Solid State Mater.* **2002**, *6*, 205.
3. Ray, S. S.; Okamoto, M. *Prog. Polym. Sci.* **2003**, *28*, 1539.
4. Ahmadi, S. J.; Huang, Y. D.; Li, W. *J. Mater. Sci.* **2004**, *39*, 1919.
5. Becker, O.; Simon, G. P. *Adv. Polym. Sci.* **2005**, *179*, 29.
6. Thostenson, E. T.; Li, C.; Chou, T.-W. *Compos. Sci. Technol.* **2005**, *65*, 491.
7. Usuki, A.; Hasegawa, N.; Kato, M. *Adv. Polym. Sci.* **2005**, *179*, 135.
8. Zeng, Q. H.; Yu, A. B.; Lu, G. Q.; Paul, D. R. *J. Nanosci. Nanotechnol.* **2005**, *5*, 1574.
9. Balazs, A. C.; Emrick, T.; Russell, T. P. *Science* **2006**, *314*, 1107.
10. Baur, J.; Silverman, E. *MRS Bull.* **2007**, *32*, 328.
11. Hunter, D. L.; Kamena, K. W.; Paul, D. R. *MRS Bull.* **2007**, *32*, 323.
12. Hussain, F.; Hojjati, M.; Okamoto, M.; Gorga, R. E. *J. Compos. Mater.* **2006**, *40*, 1511.
13. Krishnamoorti, R. *MRS Bull.* **2007**, *32*, 341.
14. Vaia, R. A.; Maguire, J. F. *Chem. Mater.* **2007**, *19*, 2736.
15. Winey, K. I.; Vaia, R. A. *MRS Bull.* **2007**, *32*, 314.
16. Paul, D. R.; Robeson, L. M. *Polymer* **2008**, *49*, 3187.
17. Zeng, Q. H.; Yu, A. B.; Lu, G. Q. *Prog. Polym. Sci.* **2008**, *33*, 191.
18. Gibson, R. F. *Compos. Struct.* **2010**, *92*, 2793.
19. Li, C.; Han, J.; Ryu, C. Y.; Benicewicz, B. C. *Macromolecules* **2006**, *39*, 3175.
20. Mackay, M. E.; Tuteja, A.; Duxbury, P. M.; Hawker, C. J.; Van Horn, B.; Guan, Z.; Chen, G.; Krishnan, R. S. *Science* **2006**, *311*, 1740.
21. Schadler, L. S.; Kumar, S. K.; Benicewicz, B. C.; Lewis, S. L.; Harton, S. E. *MRS Bull.* **2007**, *32*, 335.
22. Li, Y.; Benicewicz, B. C. *Macromolecules* **2008**, *41*, 7986.
23. Akcora, P.; Liu, H.; Kumar, S. K.; Moll, J.; Li, Y.; Benicewicz, B. C.; Schadler, L. S.; Acehan, D.; Panagiotopoulos, A. Z.; Pryamitsyn, V.; Ganesan, V.; Ilavsky, J.; Thiyagarajan, P.; Colby, R. H.; Douglas, J. F. *Nat. Mater.* **2009**, *8*, 354.
24. Wu, Y.; Zhang, J.; Zhao, H. *J. Polym. Sci. A1* **2009**, *47*, 1535.
25. Maillard, D.; Kumar, S. K.; Fragneaud, B.; Kysar, J. W.; Rungta, A.; Benicewicz, B. C.; Deng, H.; Brinson, L. C.; Douglas, J. F. *Nano Lett.* **2012**, *12*, 3909.
26. Kumar, S. K.; Jouault, N.; Benicewicz, B.; Neely, T. *Macromolecules* **2013**, *46*, 3199.
27. Odegard, G. M.; Clancy, T. C.; Gates, T. S. *Polymer* **2005**, *46*, 553.
28. Strawhecker, K. E.; Manias, E. *Chem. Mater.* **2000**, *12*, 2943.
29. Strawhecker, K. E.; Manias, E. *Macromolecules* **2001**, *34*, 8475.
30. Chang, J.-H.; Jang, T.-G.; Ihn, K. J.; Lee, W.-K.; Sur, G. S. *J. Appl. Polym. Sci.* **2003**, *90*, 3208.
31. Yeh, J.-M.; Yu, M.-Y.; Liou, S.-J. *J. Appl. Polym. Sci.* **2003**, *89*, 3632.
32. Yu, Y.-H.; Lin, C.-Y.; Yeh, J.-M.; Lin, W.-H. *Polymer* **2003**, *44*, 3553.
33. Döppers, L.-M.; Breen, C.; Sammon, C. *Vib. Spectrosc.* **2004**, *35*, 27.

34. Grunlan, J. C.; Grigorian, A.; Hamilton, C. B.; Mehrabi, A. R. *J. Appl. Polym. Sci.* **2004**, *93*, 1102.
35. Wang, L.-P.; Wang, Y.-P.; Zhang, F.-A. *Polym. Polym. Compos.* **2005**, *13*, 839.
36. Adoor, S. G.; Sairam, M.; Manjeshwar, L. S.; Raju, K. V. S. N.; Aminabhavi, T. M. *J. Membrane Sci.* **2006**, *285*, 182.
37. Gaume, J.; Taviot-Gueho, C.; Cros, S.; Rivaton, A.; Thérias, S.; Gardette, J.-L. *Sol. Energ. Mat. Sol. C* **2012**, *99*, 240.
38. Ploehn, H. J.; Liu, C. *Ind. Eng. Chem. Res.* **2006**, *45*, 7025.
39. Greenland, D. J. *J. Coll. Sci. Imp. U. Tok.* **1963**, *18*, 647.
40. Emerson, W. W.; Raupach, M. *Aust. J. Soil Res.* **1964**, *2*, 46.
41. Theng, B. K. G. *Clay Clay Miner.* **1970**, *18*, 357.
42. Suzuki, K.; Mori, T.; Kawase, K.; Sakami, H.; Iida, S. *Clays Clay Miner.* **1988**, *36*, 147.
43. Carrado, K. A.; Thiyagarajan, P.; Elder, D. L. *Clays Clay Miner.* **1996**, *44*, 506.
44. Luckham, P. F.; Rossi, S. *Adv. Colloid Interface Sci.* **1999**, *82*, 43.
45. de Bussetti, S. G.; Ferreiro, E. A. *Clays Clay Miner.* **2004**, *52*, 334.
46. Nielsen, L. E. *J. Macromol. Sci.* **1967**, *A1*, 929.
47. Cussler, E. L.; Hughes, S. E.; Ward, W. J.; Rutherford, A. *J. Membr. Sci.* **1988**, *38*, 161.
48. Falla, W. R.; Mulski, M.; Cussler, E. L. *J. Membr. Sci.* **1996**, *119*, 129.
49. Lape, N. K.; Nuxoll, E. E.; Cussler, E. L. *J. Membr. Sci.* **2004**, *236*, 29.
50. Russel, W. B.; Saville, D. A.; Schowalter, W. R. Colloidal Dispersions; Cambridge University: Cambridge, **1989**.
51. Fleer, G.; Cohen Stuart, M. A.; Scheutjens, J. M. H. M.; Cosgrove, T.; Vincent, B. Polymers at Interfaces; Chapman & Hall: London, **1993**.
52. Chaplain, V.; Janex, M. L.; Lafuma, F.; Graillat, C.; Audebert, R. *Colloid Polym. Sci.* **1995**, *273*, 984.
53. Backfolk, K.; Rosenholm, J. B.; Husband, J.; Eklund, D. *Colloids Surf. A* **2006**, *275*, 133.
54. Tadros, T. F. *Colloids Surf.* **1986**, *18*, 137.
55. Wu, W.-L.; Shibayama, M.; Roy, S.; Kurokawa, H.; Coyne, L. D.; Nomura, S.; Stein, R. S. *Macromolecules* **1990**, *23*, 2245.
56. Willcox, P. J.; Howie, D. W., Jr.; Schmidt-Rohr, K.; Hoagland, D. A.; Gido, S. P.; Pudjijanto, S.; Kleiner, L. W.; Venkatraman, S. *J. Polym. Sci. Polym. Phys.* **1999**, *37*, 3438.
57. Kanaya, T.; Takahashi, N.; Takeshita, H.; Ohkura, M.; Nishida, K.; Kaji, K. *Polym. J.* **2012**, *44*, 83.
58. Thompson, J. W.; Stretz, H. A.; Arce, P. E.; Gao, H.; Ploehn, H. J.; He, J. *J. Appl. Polym. Sci.* **2012**, *126*, 1600.
59. Cui, Y.; van Duijneveldt, J. S. *Langmuir* **2010**, *26*, 17210.
60. Rossi, S.; Luckham, P. F.; Tadros, T. F. *Colloids Surf. A* **2003**, *215*, 1.
61. Ploehn, H. J.; Russel, W. B.; Hall, C. K. *Macromolecules* **1988**, *21*, 1075.
62. Ploehn, H. J.; Russel, W. B. *Macromolecules* **1989**, *22*, 266.
63. Ploehn, H. J.; Russel, W. B. *Adv. Chem. Eng.* **1990**, *15*, 137.
64. Sapalidis, A. A.; Katsaros, F. K.; Steriotis, T. A.; Kanellopoulos, N. K. *J. Appl. Polym. Sci.* **2012**, *123*, 1812.
65. Chibowski, S.; Paszkiewicz, M.; Krupa, M. *Powder Technol.* **2000**, *107*, 251.